Fuel Processing Technology 249 (2023) 107860

Contents lists available at ScienceDirect

Fuel Processing Technology

journal homepage: www.elsevier.com/locate/fuproc

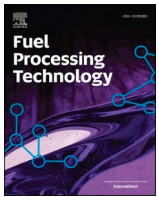

Water-assisted HDO of biomass model compounds enabled by Ru-based catalysts

S. Carrasco-Ruiz [a], S. Parrilla-Lahoz [a,b], J.L. Santos [c], A. Penkova [a], J.A. Odriozola [a,b], T.R. Reina [a,*], L. Pastor-Perez [a]

[a] Inorganic Chemistry Department and Materials Science Institute, University of Seville-CSIC, Sevilla 41092, Spain
[b] Department of Chemical and Process Engineering, University of Surrey, Guildford GU2 7XH, United Kingdom
[c] King Abdullah University of Science and Technology, Thuwal, Saudi Arabia

ARTICLE INFO

Keywords:
Biomass upgrading
HDO
Novel catalytic routes
Ru catalysts

ABSTRACT

Biofuels upgrading gathering momentum in view of the gradual depletion of fossil fuels and the pursuit of renewable energy sources to mitigate global warming. Hydrodeoxygenation (HDO) is a key reaction in the upgrading of bio-oil to produce hydrocarbon fuels or high-value chemicals. Oxygen removal in bio-oil increases its calorific value, improve thermal and chemical stability, reduce corrosiveness, etc., making the upgraded bio-oil suitable as a fuel or blending fuel. However, the dependence on high-pressure hydrogen is a serious disadvantage, as it is an expensive resource whose use also poses safety concerns. In this scenario, we propose a pioneering route for model biomass compounds upgrading via *H_2-free* HDO. Herein we have developed multifunctional catalysts based on Ru and ceria supported on carbon able conduct the hydrodeoxygenation reaction using water as hydrogen source. We found that cerium oxide improves ruthenium metallic dispersion and the overall redox properties of the multicomponent system leading to enhanced catalytic performance. Along with the successful catalytic formulation we identify 300 °C as an optimal temperature validating the *H_2-free* HDO route for bio-compounds upgrading.

1. Introduction

The polluting nature of fossil fuels has led to a shift from fossil fuels to renewable energies in recent years. The current scenario indicates that, although increasingly used, renewable energies are still far from becoming a primary resource for one simple reason: they are not yet economically profitable compared to fossil fuels. Thus, the global energy market is still dominated by fossil fuels, accounting for >80% of energy consumption and, in addition, three-quarters of global greenhouse gas (GHG) emissions come from the burning of this fossil fuels for energy [1].

In this vein, placing renewable energies in a competitive position with respect to fossil fuels necessarily involves minimising production cost as well as reducing environmental impact. Based on this premise, biomass, and in particular biomass residues, represent a promising substitute for fossil fuels. Biomass, the biological material derived from living or relative living organisms, owns unique advantages, such as abundance, low price, diversity and wide distribution, over other renewable energy sources [2]. Moreover, biomass is the only renewable source from which liquid fuels can be obtained [3]. But undoubtedly, the key point of this energy source is that biofuels derived from biomass are carbon neutral in nature considering the fact that the CO_2 released by their combustion is neutralised by the CO_2 utilization occurring naturally in plants, accordingly, not affecting the net CO_2 level in the atmosphere [4,5].

Thermochemical process, such as pyrolysis and gasification, are the well-stablished biomass processing technologies to produce biofuels and biochemicals [6,7]. Nonetheless, it should be noticed that high oxygen content in biofuels leads to several shortcomings compared to conventional diesel fuel, such as low heating value, engine compatibility issues, or poor stability, making it unsuitable as complete replacement of diesel [8,9]. These adverse characteristics of pyrolytic bio-oil are genuinely problematic in lignin-derived bio-oils which are the most promising alternatives given the high proportion of lignin in raw biomass compared to other components such as cellulose and hemicellulose [10].

In general, lignin-derived pyrolytic oils contain a dominating

* Corresponding author.
E-mail address: tramirez@us.es (T.R. Reina).

https://doi.org/10.1016/j.fuproc.2023.107860
Received 10 April 2023; Received in revised form 15 May 2023; Accepted 24 May 2023
Available online 2 June 2023

fraction of phenolics, yield 25–40 wt% (with 7–11 wt% monomers) derived from fast pyrolysis of lignin [11]. In catalytic studies to understand the mechanistic aspects as well as the fundamental parameters of catalyst design, monomeric models of lignin fragments are often used [12].

Hence, bio-oil upgrading is an essential process necessary to covert bio-oil into a deoxygenated fuel with physicochemical characteristics comparable to those exhibited by petroleum oils [13]. In this sense, there are several reaction pathways to remove the oxygen from bio-oil:

1) Decarbonylation (DCN): removal of oxygen in the form of CO

$$R-COOH \rightarrow R-H+CO+H_2O$$

2) Decarboxylation (DCX): elimination of oxygen in the form of CO_2

$$R-COOH+H_2 \rightarrow R-H+CO_2$$

$$R-COOH \rightarrow R^{'}-H+CO_2$$

3) Hydrodeoxygenation (HDO): withdrawal of oxygen in the form of H_2O

$$R-OH+H_2 \rightarrow R-H+H_2O$$

R = saturated alkyl/aryl group R' = unsaturated alkyl group

Among these options, HDO exhibits remarkable advantages, such as low reaction temperature, high oxygen removal efficiency and preservation of the carbon number in the structure of products [14]. While these advantages are compelling, from an economic point of view, DCX and DCN are more attractive since they own the advantage of a reduced or zero hydrogen gas consumption [15,16]. Specifically, HDO of bio-oil or bio-oil model compounds is generally carried out at a relatively low reaction temperature (200–400 °C) and high hydrogen pressure in a batch autoclave reactor (4–20 MPa) or a continuous fixed bed reactor (5–10 MPa) [17].

Thus, in order to deploy HDO technology on a commercial scale, it is necessary to overcome the bottleneck of dependence on high-pressure hydrogen, an expensive resource whose use also raises safety concerns. Besides, current large-scale commercial technologies for hydrogen production (i.e., natural gas reforming) involves a heavy carbon dioxide emission penalty which limits the process sustainability [18]. In this regard, the so-called *H_2-free* HDO process is a highly desired approach to upgrade oxygenated bio-oil mixtures by suppressing external hydrogen supply [19]. As depicted in Fig. 1, this process utilises water as reaction media and a multifunctional catalyst to remove oxygen from the organic fraction and deliver deoxygenated hydrocarbons [20–22].

This is indeed a very challenging process, as it requires a multifunctional catalyst capable of activating water and hydrocarbon molecules to subtract hydrogen and simultaneously catalyse the hydrogen transfer and the deoxygenation processes in a single step. These materials must have a high specific surface area, a large pore volume to facilitate diffusion of the reactants, acidic properties for the dehydration reaction and redox metal sites for the hydrogenation and dehydrogenation reactions. Moreover, metal oxide promoters capable of inducing water dissociation are necessary for generating hydrogen in situ. Some potential catalytic systems for *H_2-free* HDO process are hierarchical zeolite or carbon-based materials doped with a metallic phase and promoted with a metal oxide redox pair active for water activation. Carbon-based materials are considered environmentally friendly catalysts [23], while hierarchical zeolites are potential supports for hydrogenation due to their accessibility and acidic properties [24].

Given with ambitious challenge posed by the design of advanced multifunctional catalysts for the *H_2-free* HDO process, model oxygenated monomeric compounds that represents fractions of the complex lignin-like bio-oil mixtures are ideal systems to conduct a fundamental study. In particular, guaiacol is the most representative, as it contains two different oxygenated groups: methoxy and phenolic groups, so it provides a simplified case suitable for studying catalytic oxygen removal [21,25]. Several studies have proposed a simplified scheme of the different pathways of guaiacol conversion according to the products obtained (Fig. 2) [26,27]. Thus, anisole and catechol are intermediates products from dehydroxylation (DHO) and demethylation (DME) respectively. Both should lead to phenol, and it is just the previous step before accomplishing full oxygen removal to yield benzene. Phenol can also be obtained by demethoxylation (DMO) of guaiacol, thus providing a third possible route to produce benzene. Another product that can be observed is o-cresol due to the transalkylation of guaiacol and the subsequent DHO process.

Under the above discussed scenario, the overriding goal of this paper

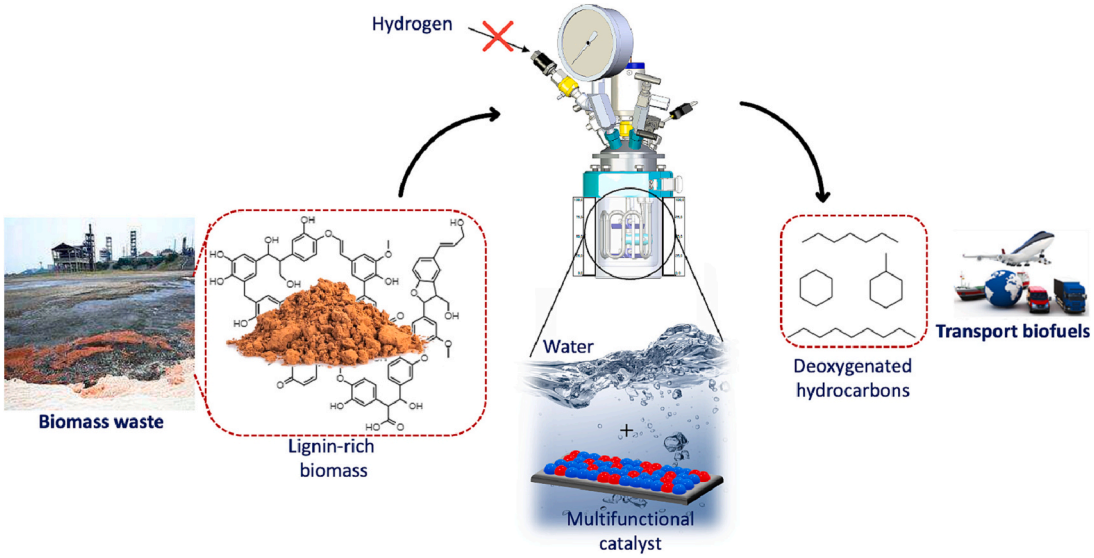

Fig. 1. Schematic overview of the H_2-free HDO process.

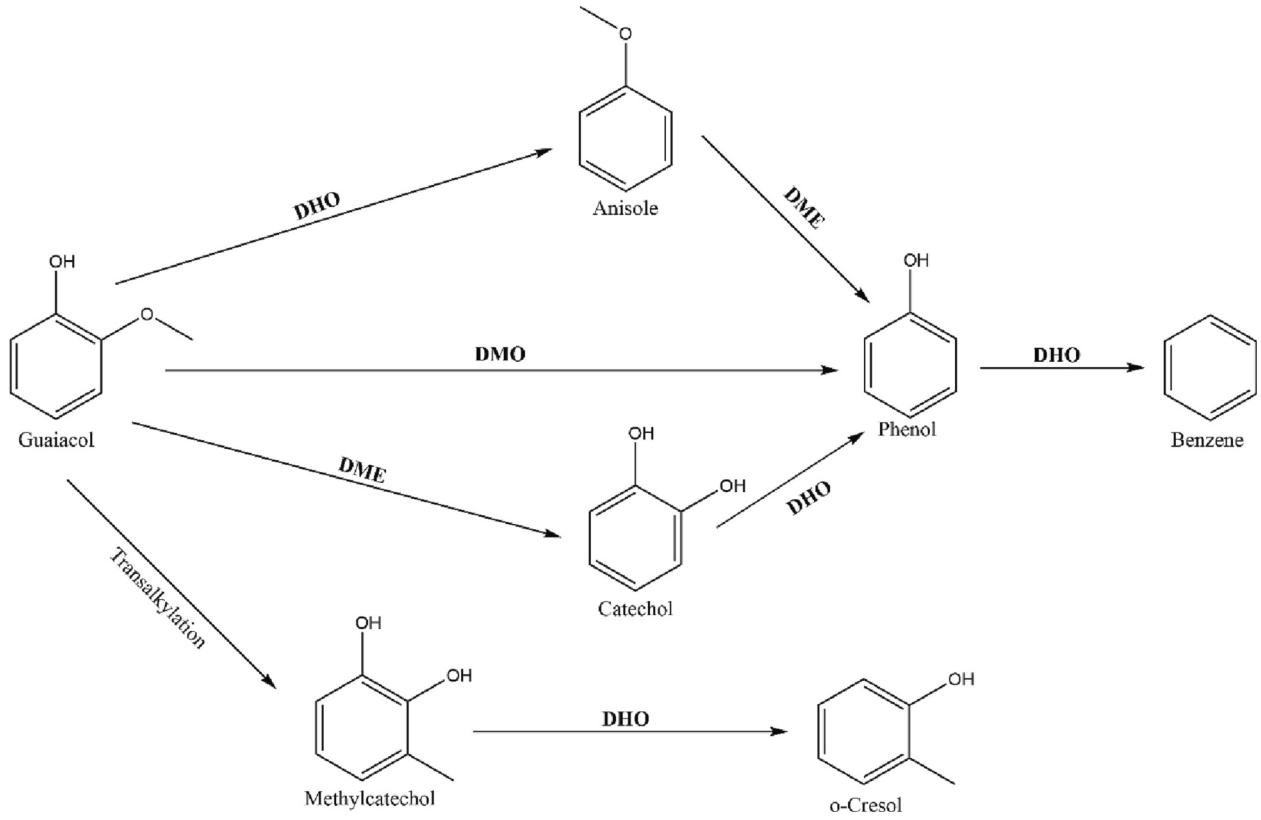

Fig. 2. Proposed reaction pathways for HDO process of guaiacol over noble metal catalysts based on previous works [28].

is to design multifunctional catalysts that can reliably facilitate HDO of guaiacol using water as hydrogen source to produce essential platform aromatic compounds (biofuels/biochemicals). We will study two activated carbon-based catalysts: a ruthenium supported catalyst and a Ru-CeO_2 dopped catalyst. The best of the two formulations will be selected and studies will be carried out on reproducibility, recyclability, and temperature screening to optimise HDO performance.

2. Materials and methods

2.1. Catalysts preparation

This work has focused on the study of two ruthenium catalytic systems supported on commercial activated carbon (AC). A commercial charcoal *NORIT* purchased from Merck was employed as the carbon support.

The first catalyst was prepared by wet impregnation, where the support was first impregnated with ruthenium (III) nitrosyl nitrate solution ($Ru(NO_3)_3(NO)$, Johnson Matthey), diluted in acetone, and then the solvent was gradually removed at reduced pressure in a rotary evaporator at 50 °C. The sample was dried at 100 °C overnight and finally calcined at 400 °C (2 °C/min rate) for 4 h under inert atmosphere conditions (50 mL/min N_2) to obtain the Ru/AC catalyst.

The second catalyst was prepared also by wet impregnation, except in this case the support was impregnated with cerium (III) nitrate hexahydrate ($Ce(NO_3)_3{\cdot}6H_2O$, Merck), diluted in acetone, and the solvent was gradually removed at reduced pressure in a rotary evaporator at 50 °C. The sample was dried at 100 °C overnight and finally calcined at 400 °C (2 °C/min rate) for 4 h under inert atmosphere conditions (50 mL/min N_2). Once this is done, the resulted Ce/AC sample was impregnated with the ruthenium precursor in a similar procedure as explained above to obtain the RuCe/AC catalyst.

In all cases, the Ru content is calculated to be 2 wt% and 20 wt% Ce for the second sample. These ratios were chosen based on previous works [29].

2.2. Characterisation techniques

The textural properties of the samples were evaluated from nitrogen adsorption-desorption isotherms at liquid nitrogen temperature in a Micromeritics Tristar II apparatus. Before analysis the samples were degassed at 250 °C for 4 h in vacuum.

X-ray diffraction technique (XRD) measurements were carried out in a X'Pert Pro PANanalytic instrument. The diffraction patterns were recorded at 40 mA and 45 kV using Cu-Kα radiation ($\lambda = 0.154$ nm). The 2θ angle was increased using a step size of 0.05° and a step time of 300 s in a range of 10 to 90°.

Scanning electron microscopy (SEM) analysis were performed in a vacuum, using a JEOL 5400 microscope equipped with an EDS analyser (Oxford Link).

High resolution transmission electron microscopy (HR-TEM) measurements were carried out using a FEI Talos F200S with a HAADF STEM detector, with a high acceleration potential of up to 200 kV.

The XPS experiments were carried out on a SPECS photoelectron spectrometer equipped with a PHOIBOS 150 MCD analyser operating with constant pass energy at 40 eV and 1.0 eV resolution. As X-ray radiation source, the Kα emission from the electron bombardment of Al target with energy $h\nu = 1486.6$ eV and bandwidth of 0.85 eV, operating at 250 W and maintaining the potential at 12.5 kV, was used. The analysis chamber operates under ultra-high vacuum conditions, with a pressure of 10^{-10} mbar.

H_2-Temperature-programmed reduction (TPR) experiments were conducted in a tube quartz reactor passing a flow 50 mL/min of 5% H_2 diluted in N_2, with a heating rate of 10 °C/min. Hydrogen consumption, water production and methane production were recorded using an on-line mass spectrometer (Pfeiffer, OmniStar GSD 301).

2.3. Evaluation of catalytic activity

The guaiacol HDO reaction were performed in a high-pressure batch reactor (Parr Series 5500 HPCL Reactor Controller). 1 wt% of guaiacol in water (0.5 g) and 0.05 g of catalyst were loaded in a 300 mL glass-lined steel vessel. To avoid any air contamination, N_2 was bubbled through the solution for 5 min under a stirring speed of 100 rpm before closing the reaction vessel. Then, the reactor was heated to the desired temperature (200 °C, 250 °C, 300 °C as required for each experiment) and hold at this temperature for four hours under a stirring speed of 300 rpm. After the reaction, the spent catalyst was recovered from the liquid by filtration, washing with ethyl acetate and followed by drying treatment at 80 °C for 12 h. The organic products were dissolved and recovered with ethyl acetate extraction.

The identification of the organic compounds produced from guaiacol HDO reaction was performed by gas chromatograph-mass spectrometry (GC–MS). Quantitative analysis was carried out with a gas chromatograph-flame ionisation detector (GC, Shimadzu; FID: Agilent cellular model). The injector temperature was held at 280 °C. The GC separation was performed using a Carboxen Packed Analytical Column (30 m × 320 μm × 0.25 μm). A split ratio of 8:1 was maintained. The analytical method consisted of holding the temperature at 50 °C for 1 min, then increased to 240 °C at a heating rate of 5 °C/min and held at this temperature for 10 min. Reactant and typical products were quantified based on the external standard method.

The conversion of guaiacol and the selectivities towards typical products (based on C mol) were calculated using *Eqs. 1 & 2*, respectively.

$$Conversion\ of\ guaiacol = \frac{n_{GUAin} - n_{GUAout}}{n_{GUAin}} \cdot 100 \quad (1)$$

$$Selectivity\ of\ product\ i = \frac{n_i \cdot N_i}{(n_{GUAin} - n_{GUAout}) \cdot N_{GUA}} \cdot 100 \quad (2)$$

where n_{GUAin}: initial mole of guaiacol; n_{GUAout}: detected mole of guaiacol in the organic phase; n_i: mole of product *i*; N_{GUA}: number of carbons in guaiacol; N_i: number of carbons in product *i*.

3. Results and discussion

3.1. Characterisation of solid catalysts

The textural properties (S_{BET}, pore size and pore volume) of the catalysts and the commercial activated carbon are summarized in Table 1. As depicted in the table, the specific surface areas of the catalysts decrease as the metal loading on the activated carbon support increases. This indicates that both Ru and CeO_2 are introduced within the support porous structure. Likewise, the pore volume (V_{pore}) follows a similar descending trend for very same reason mentioned above. The pore width (D_{pore}), however, is not strongly altered, suggesting that the pore size distribution remains homogeneous. In any case, all the studied materials present a high surface area.

In addition, the adsorption and desorption isotherms curves have been obtained for both catalysts as shown in *Fig. S1*. According to IUPAC classification, six isotherm types are usually found in catalyst characterisation, and each isotherm shape depends directly on the solid porous texture [30]. In our case, these isotherms correspond to a *Type I.b* isotherm, suggesting that the AC and solid catalysts are highly microporous. The hysteresis observed after $P/P_0 > 0.4$ corresponds to a slight presence of mesopore. Besides, there is also a classification of the type of hysteresis, being the *Type H4* found in our isotherms. This kind of hysteresis is characteristic of solids consisting of aggregates or agglomerates of particles forming slit shaped pores, with uniform size and shape.

Table 1
Textural properties of the catalysts.

Sample	S_{BET} (m^2/g)	V_{pore} (cm^3/g)	D_{pore} (Å)
NORIT Carbon	837	0.20	26.6
Ru/AC	789	0.18	27.2
Ce/AC	484	0.11	28.6
RuCe/AC	479	0.11	28.7

The crystalline structure of the activated carbon and the prepared catalysts were analysed by means of X-Ray Diffraction (Fig. 3). The first diffractogram corresponds to the commercial NORIT carbon. As we can see, the XRD pattern is mostly amorphous with distinguishable crystalline domains corresponding to the (002), (100) and (110) planes (diffraction peaks at 24.8, 43.0 and 79.8 respectively) [31]. However, an abundance of crystalline inorganic constituents is evident in the NORIT AC support. These could be associated with some impurities such as calcite or boron nitride. Other studies have also reported the presence of impurities in this kind of samples [32]. The Ru/AC diffractogram is quite similar to the activated carbon one. In fact, no crystalline phases of ruthenium were detected. This indicates a high degree of dispersion of the active phase on the support. Finally, the RuCe/AC diffractogram shows intensely the diffraction lines of cerium oxide [33,34]. The crystalline planes correspond to typical reflections on the CeO_2 fluorite cubic cell.

The morphology of the activated carbon is shown in the SEM micrographs provided in *Fig. S2*. NORIT carbon presents uneven cylindrical pores with small globules and sharp indentations on the wall surface and an irregular discontinuous surface consisting of small cavities and rough surfaces. Cavities and voids noted may be due to activation processes and activating agents [35]. On the other hand, we acknowledge that the magnification factor applied is not sufficient to examine the exact micropores in the porous matrices of the samples, but this is beyond the present study.

Analysing the distribution of elements in the different mappings of SEM-EDX analysis (Fig. 4), we can confirm that both Ru and Ce are well dispersed and homogeneously distributed on the surface of the catalysts, corroborating a successful synthesis for both samples. In addition, the EDX analysis showed the presence of K in the samples, which is an impurity of the carbon as reported in other studies [32]. The presence of impurities may sound a priori as a trouble for the sample composition but in this very case, the presence of potassium turns a problem into a virtue since alkali atoms are effective promoters to activate C—O bonds. Indeed, our team has demonstrated the beneficial effect of Cs and K as promoters to activate CO_2 [36,37]. Hence, we will benefit of K-presence

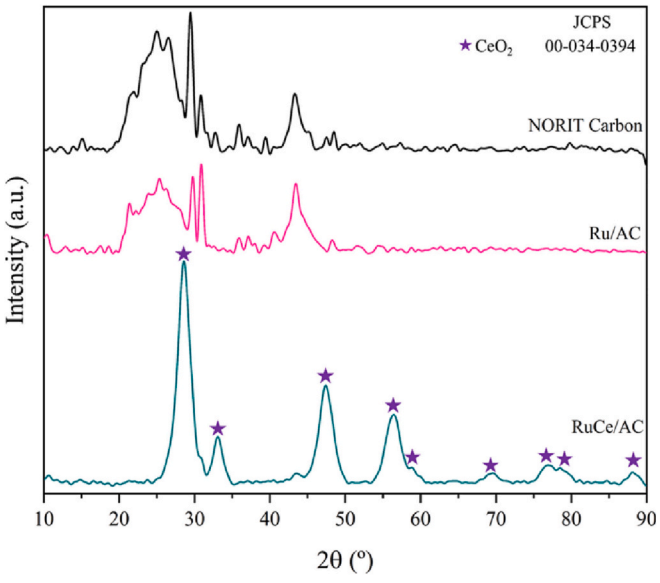

Fig. 3. XRD of NORIT carbon and prepared catalysts.

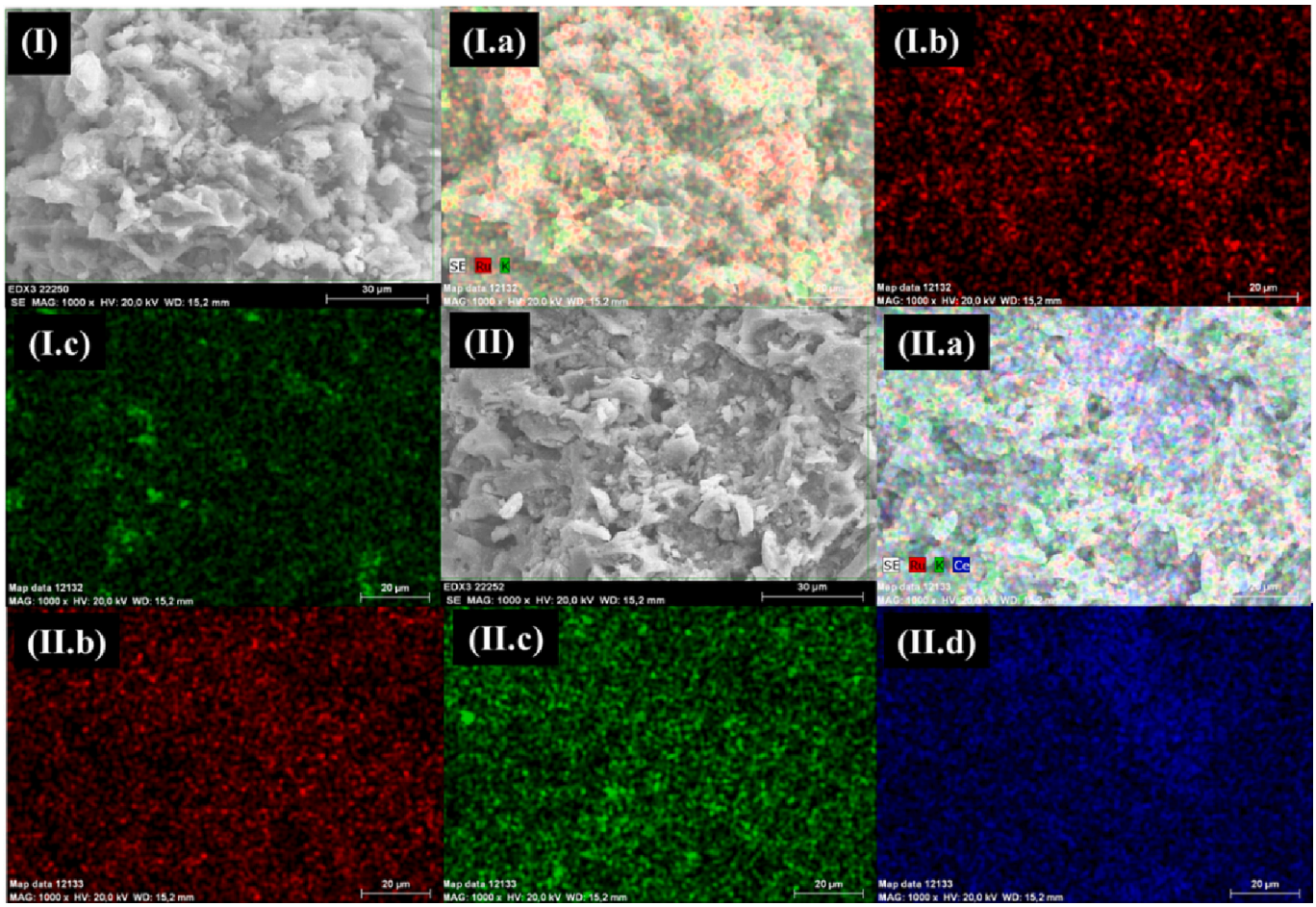

Fig. 4. SEM micrographs of both calcined catalysts: (I) Ru/AC and (II) RuCe/AC; where (a) general mapping; (b) Ru mapping; (c) K mapping; (d) Ce mapping.

in the original carbon support to favor C—O bond breaking in our complex HDO reaction.

To gather further insights in the morphological and structural undertraining of our samples High Resolution Transmission Electron Microscopy (HR-TEM) analyses were performed. As we can see in Fig. 5, thanks to the high resolution of this characterisation technique, we can analyse the interplanar distance of the different crystalline phases found in the samples. Interestingly, both sample Ru/AC and sample RuCe/AC show the interplanar distance of the metallic Ru (101) plane. Although it is the only plane detected, it matches the most intense reflection of the hexagonal structure of ruthenium. Hence our sample are composed by reduced Ru species without the need for pre-reduction/activation treatment with hydrogen [38]. This is a remarkable advantage when a realistic process in envisage since eliminating the catalyst conditioning could represent significant OPEX savings. On the other hand, the second sample shows the interplanar distance of cubic cerium oxide (111).

The study of the average particle size of ruthenium in both catalysts exhibits a Gaussian distribution (*Fig. S3*). This type of distribution shows that the metal dispersion is broadly homogeneous. While it is true that the distribution is similar in both samples, in the case of the Ru/AC catalyst the average ruthenium particle size is 3.9 nm while in the RuCe/AC catalyst it is close to 3 nm.

Fig. 6 shows representative STEM of Ru/AC catalyst. As we can see, the dispersion of ruthenium metal on carbon can be observed in both brightfield (BF) and darkfield (HAADF) micrographs. The Energy Dispersive X-Rays Spectroscopy (EDS) of this sample indicates the presence of carbon, oxygen, silicon, and ruthenium, as well as two unassigned bands. One of metallic copper (from the grid), and the other of potassium in fair agreement with our SEM and XRD analysis revealing impurities within the commercial carbon appear. Quantitative analysis determined that the mass fractions of silicon and potassium are 0.4 wt% and 4.6 wt% respectively.

The same analysis was performed on the RuCe/AC sample (Fig. 7). As in the previous case, the same elements are observed by EDS analysis, resulting in a silicon and potassium mass fractions of 1.1 wt% and 5.5 wt %. As for the dispersion of ruthenium on the catalyst, a good dispersion of this metallic phase is observed. However, it should be highlighted that ruthenium is dispersed preferentially on cerium than on carbon, as can be clearly seen in Fig. 6.*d* and Fig. 6.*e* [39].

The chemical composition of the surface was determined from the area of the peaks C1s + Ru3d(+Ce4s), O1s, Ru3p, K2p and S2p considering the relative sensitivity factors of each peak (RSF). For the correction of the charge effect of the samples, the C1s peak was used as internal standard, fixing it at 284.6 eV. For the correction of the background signal, the Sharley line (background) was used. Fig. 8.*a* represents the general spectra of both samples, where we can observe C, Ru, Ce and O peaks clearly [40]. In addition, significant K content is detected in the surface and as mentioned before this is indeed an advantage given the role of K as promoter for this reaction.

Table 2 shows the atomic percentage of the peaks of the main species observed. As can be seen, the Ru $3p_{3/2}$ surface percentage is higher for the second catalyst, suggesting a better dispersion of the noble metal with the addition of cerium, in fair agreement with the TEM study. On the other hand, the potassium content is quite similar in both samples. Finally, in Fig. 8.*b* it can be seen that the shape of the spectra of the O1s zone in both samples is different due to the contribution of different species with different ratios [41]. In both samples, oxygen species from metal oxides (lattice oxygen) were detected at 529.3 ± 0.3 eV, metal

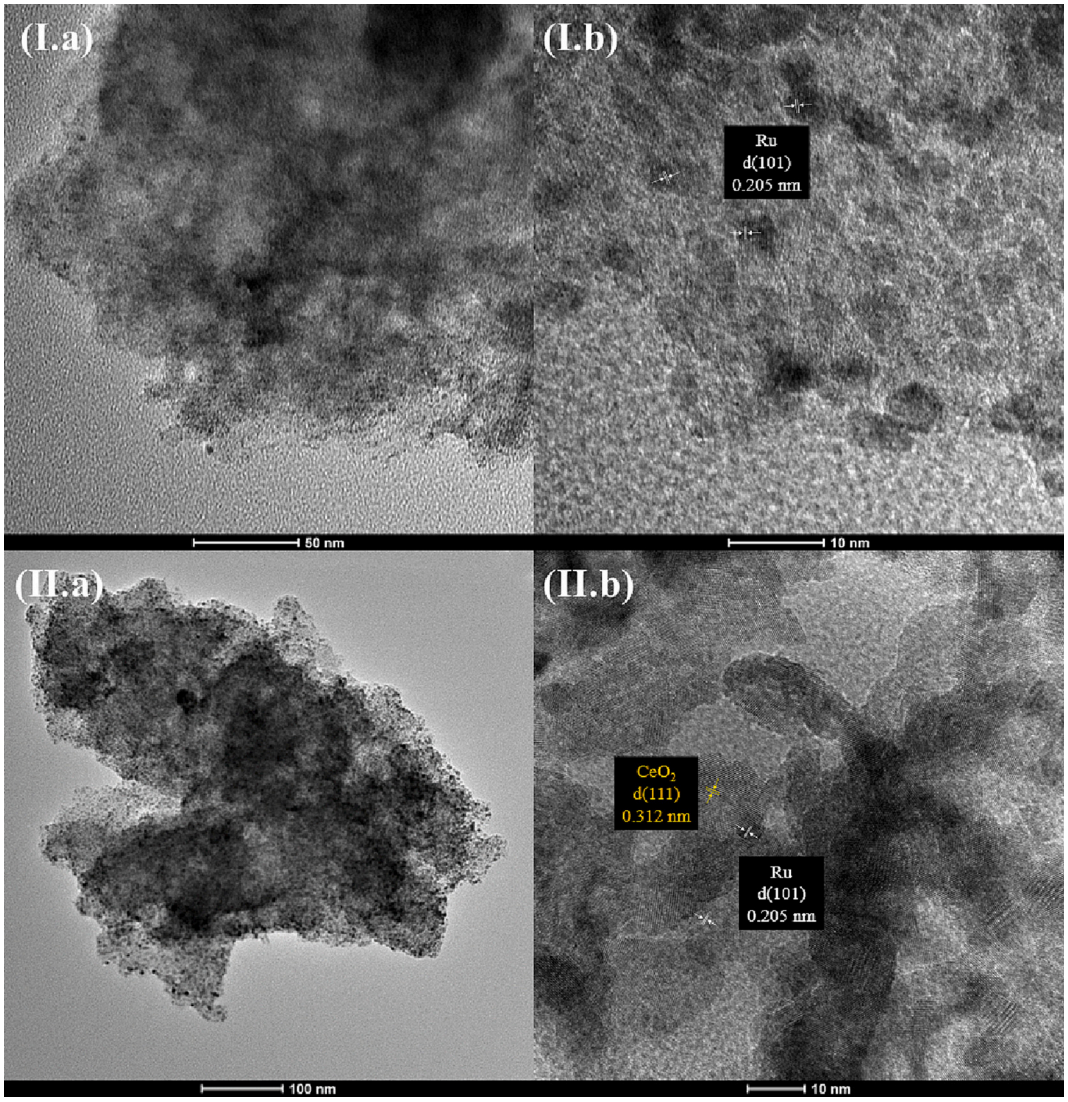

Fig. 5. Selected HR-TEM micrographs of both calcined samples: (I) Ru/AC and (II) RuCe/AC.

carbonates and hydroxyls at 531.1 ± 0.1 eV and oxygen of organic origin at 532.7 ± 0.2 eV. In addition, in the Ru/AC sample, the presence of H_2O.

Analysing the proportion of each species, there is twice as much lattice oxygen in the sample with cerium, which is logical due to the contribution of one more oxide in the composition of the catalyst. However, the peak areas of metal carbonates and hydroxyls are quite similar. Likewise, we observe that the area of organic oxygen is greater in the catalyst without cerium, where H_2O is also detected, which means an increase of *cus* centres, thus justifying a greater adsorption of adventitious carbon contamination for this sample.

A general idea of the redox features and the metal-support interaction was gathered by Temperature Programmed Reduction (TPR) analysis. The TPR profiles obtained for both catalysts are presented in Fig. 9. As evidenced in the first graph, two reduction zones can be distinguished. The first reduction occurs at 150 °C approximately and it is where the reduction of the oxidised ruthenium species (RuO_x) takes place. The second hydrogen consumption occurs between 300 and 550 °C, where carbon methanation occurs in the presence of hydrogen [42]. The addition of cerium generates a slightly more complex reduction profile. In Fig. 9.*b*, three different reduction zones are identified. The first region occurs between 100 and 150 °C, where ruthenium reduction proceeds as above, accompanied by the reduction of surface Ce^{4+} to Ce^{3+} together with Ru reduction [43]. This is in line with the TEM results discussed above, as ruthenium is preferentially dispersed on cerium, giving rise to a spill-over phenomenon upon reduction [44,45]. Carbon methanation takes place again at around 300 °C, but in this case, it is accompanied in the last reduction zone by the reduction of the remaining cerium at a temperature of about 600 °C.

We can therefore deduce that the addition of cerium decreases the reduction temperature of ruthenium although carbon methanation still occurs in the same temperature range. Cerium is not completely reduced at low temperature, but temperatures above 500 °C are necessary to reduce it completely, thus preserving the redox pair Ce^{3+}/Ce^{4+} available at the reaction temperature.

3.2. Catalytic activity

Selected calcined samples were initially tested at 300 °C which is close to safety limit of the pressurised vessel. As shown in Fig. 10, both catalysts display a mayor level of conversion compared with the blank (non-catalytic reaction) doubling conversion up to 44% conversion. The selectivity of both samples leads to intermediate compounds being catechol the dominant product. Catechol despite retaining two oxygen, is one of the intermediates that eventually lead to more advanced products [22]. The most advanced product obtained is phenol,

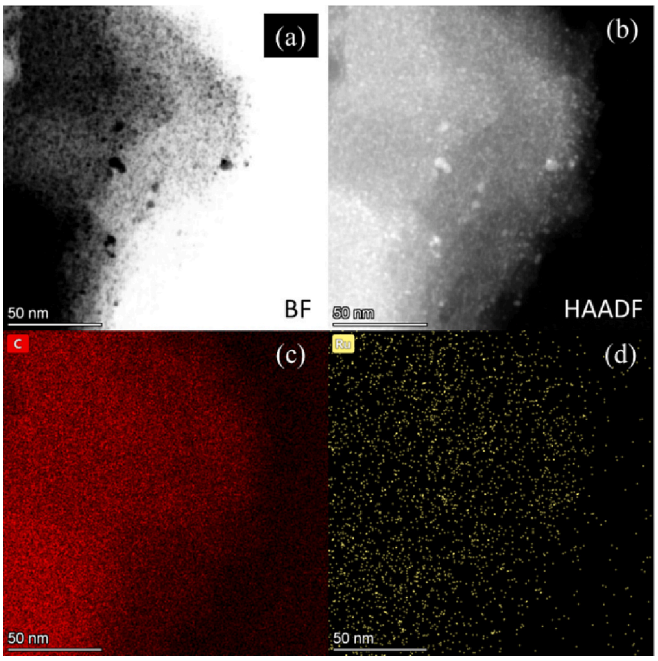

Fig. 6. Representative STEM of Ru/AC catalyst where (a) Bright Field, (b) High Annular Angle Dark Field, (c) Carbon, (d) Ruthenium.

indicating C—O cleavage is well favoured in these systems. Comparing both catalysts, we can see that RuCe/AC presents enhanced selectivity towards targeted compounds maintaining the conversion. Thus, we chose this formulation as the most promising for further tests.

It is interesting to study the catalysts recyclability to check the stability of the designed catalysts for multiple catalytic runs. For this purpose, two reaction cycles under the same conditions were studied using the catalyst recovered from the first cycle as departing material for the second run. As shown in *Fig. S4*, although the conversion decreases slightly, the selectivity results are quite promising. Thus, we can conclude that the catalyst sufficiently maintains its activity in successive reactions.

Finally, the reaction was tested at lower temperatures in attempt to lower the energy requirements of the reaction. Reaction runs at 200 and 250 °C for 4 h using the RuCe/AC sample were conducted (Fig. 11). The results show that the best condition to perform this reaction is at 300 °C, obtaining a higher conversion and selectivity than those obtained at lower temperatures. At lower temperatures, conversion to anisole, another intermediate product from the hydrogenation of C(sp^2)-OH bonds, is observed. Although it is true that, comparing anisole and catechol, the former is the more desirable product as it has only one oxygen in its composition, its low selectivity plus the low conversion obtained considerably reduce the advantages of doing the reaction at lower temperature. In addition, the selectivity to the more advanced compound, phenol, is much higher in the reaction carried out at 300 °C.

The recovered catalysts were characterised by X-ray diffraction (*Fig. S5*). We observe that the crystalline structure of the catalyst is not affected during reaction despite the relatively harsh reaction conditions (high pressure, high temperature and the presence of water). This explains the satisfactory recyclability results, indicating the structural robustness of our multicomponent catalysts for H_2-free HDO reactions.

Having validated the activity and recyclability of our catalysts in the innovative *H_2-free* HDO strategy the obvious questions is: How do they compare in terms of performance to standard HDO routes? Table 3 includes a catalytic performance comparison between traditional HDO and the *H_2-free* HDO process assisted by water. Herein, we can appreciate that it is possible to achieve total conversion of guaiacol and further deoxygenated products using high-pressure bottled hydrogen as H_2 source. Nevertheless, high-pressure hydrogen is the "Achilles heel" of this process due to all the drawbacks already commented in the introduction section. Our catalysts reached highly commendable levels of conversion and selectivity ruling out external hydrogen supply. Despite we still need further catalysts and perhaps process design improvements

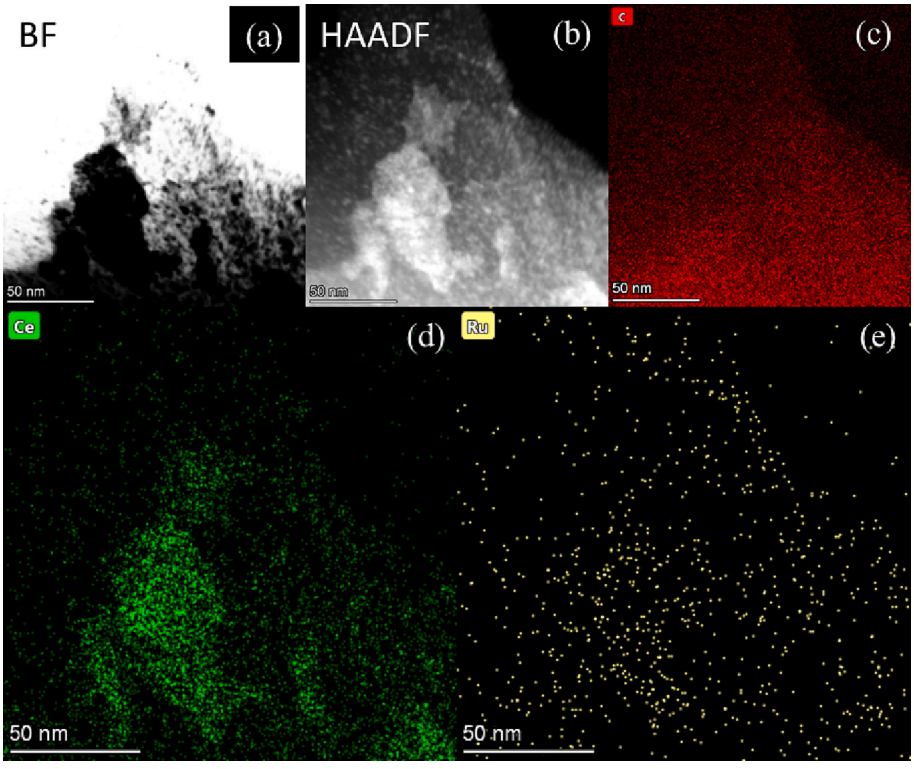

Fig. 7. Representative STEM of RuCe/AC catalyst where (a) Bright Field, (b) High Annular Angle Dark Field, (c) Carbon, (d) Cerium, (e) Ruthenium.

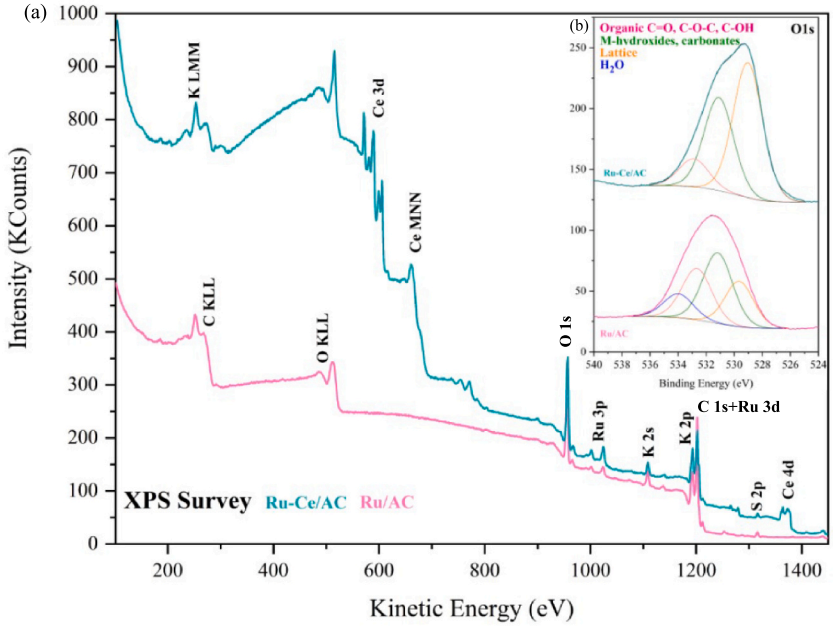

Fig. 8. XPS: (a) General spectra; (b) O 1 s spectra for both catalysts.

Table 2
Atomic percentages of the assigned species in both catalysts.

Sample	C 1 s + Ru 3d (+Ce 4 s)	Ru 3p3/2	K 2p	Ce 3d	O 1 s
Ru/AC	69.8	1.5	7.0	–	21.7
RuCe/AC	54.8	2.9	6.2	5.3	30.8

to hit the same performance levels than those of the standard route, our results evidence the potential of this economically and environmentally appealing alternative for bioresources upgrading.

4. Conclusions

This work showcases a catalytic solution to hydrogen dependence in biomass processing routes by implementing a multifunctional catalyst capable of producing hydrogen in situ from the reaction medium while catalysing the process. The result is the so called the *H_2-free* HDO process a potential novel route for biofuel production. Herein, a ruthenium-based catalyst supported on a commercial active carbon has been prepared and tested in biomass model compounds upgrading via *H_2-free* HDO, and the effect of the addition of a promoter such as cerium oxide was also studied. Indeed our TEM data reveals how cerium benefits ruthenium metallic dispersion, resulting in improved redox properties, as corroborated by TPR. The catalytic behaviour of the studied systems is highly commendable with conversion levels over 40% and displaying selectivity towards phenol as an advanced reaction product. Very importantly our multicomponent catalysts have been proven stable despite the harsh reaction conditions with no modification of the crystalline structure nor carbon deposits nucleation during the reaction. Certainly, there is room for further improvements to match the conversion levels of standard HDO routes, however we shall emphasise that our processing strategy rules out external hydrogen input in the reactor thus making significant impact in process costs reductions and brings remarkable safety advantages. In any case, our work evidences the key role played by advanced heterogeneous catalysis to deliver the next generation of biofuels in the context of a circular economy.

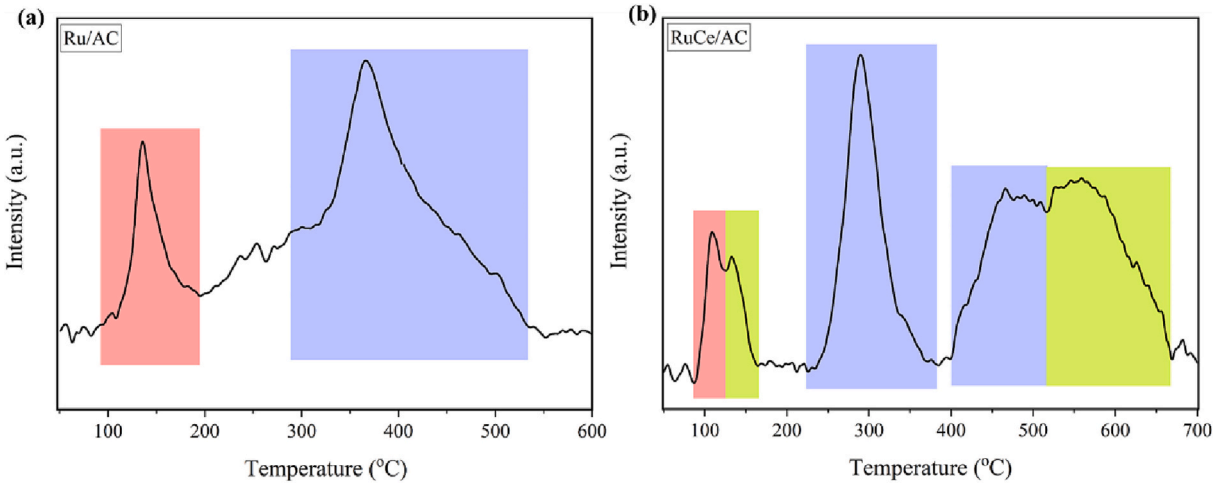

Fig. 9. H_2-TPR profiles of: (a) Ru/AC; (b) RuCe/AC.

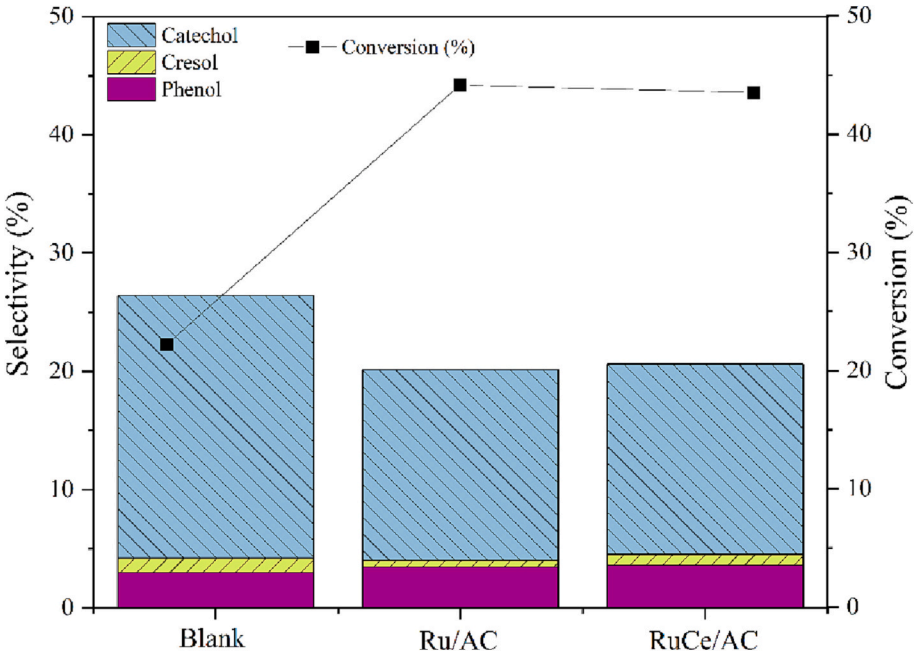

Fig. 10. Conversion at 300 °C during 4 h over Ru/AC and RuCe/AC.

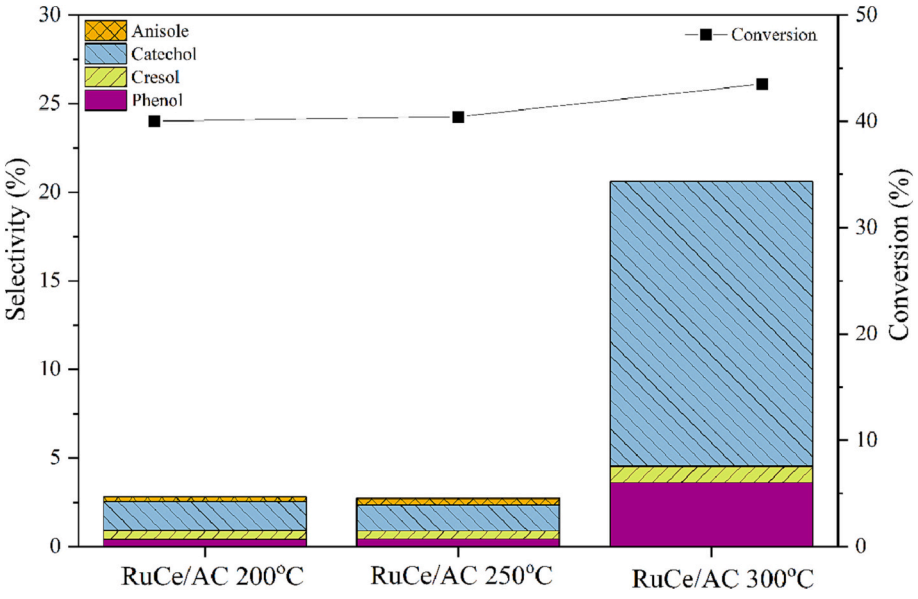

Fig. 11. Temperature screening of HDO of guaiacol over RuCe/AC catalysts.

Table 3
Catalytic performance comparison of traditional and water-assisted HDO. (CHO cyclohexanol; PHE phenol; CHE cyclohexane; CAT catechol).

Catalyst	H_2 source	Temp. (°C)	Time (min)	Conversion (%)	Major product	Selectivity (%)	Ref.
Ru/TiO_2	10 bar H_2	240	60	71.7	CHO	51	[46]
Pt/SBA-15	12 bar H_2	230	400	84.0	PHE	23	[47]
Pt-Ga/SBA-15	12 bar H_2	230	400	100	PHE	32	[47]
Ni@C	20 bar H_2	240	240	97.8	CHO	55	[48]
Pt/HBeta	40 bar H_2	250	120	>90%	CHE	45	[49]
Rh/ZrO_2	70 bar H_2	300	240	100	CHE	N/A	[50]
$NiZr_2O/Gr\text{-}n$	H_2O	300	240	52.4	CAT	11	[51]
$NiMo/CeO_2 - C$	H_2O	250	240	18.0	CAT	16	[52]
Ru/AC	H_2O	300	240	44.0	CAT	16	[*]
RuCe/AC	H_2O	300	240	43.0	CAT	17	[*]
*This work							

Authors statement

Authors declare equal contributions to this manuscript.

Funding

Authors would like to acknowledge financial support from grants PID2019-108502RJ-I00 and IJC2019-040560-I, both funded by MCIN/AEI/10.13039/501100011033 and by ESF Investing in your future. This research was also partially funded by the Junta de Andalucia PAIDI2020 programme through the CLEVER-BIO project P20_00667 and NICER-BIOFUELS project PLEC2021-008086 sponsored by MCIN/AEI/10.13039/501100011033 Next Generation Europe. S.C.R would also like to acknowledge Spanish Ministry of Science for his FPU grant (FPU21/04873).

Declaration of Competing Interest

The authors declare that they have no known competing financial interests or personal relationships that could have appeared to influence the work reported in this paper.

Data availability

Data will be made available on request.

Appendix A. Supplementary data

Supplementary data to this article can be found online at https://doi.org/10.1016/j.fuproc.2023.107860.

References

[1] H. Ritchie, M. Roser, P. Rosado, Energy, Our World in Data. https://ourworldindata.org/energy, 2020 (accessed June 7, 2022).
[2] L. Hu, L. Lin, Z. Wu, S. Zhou, S. Liu, Recent advances in catalytic transformation of biomass-derived 5-hydroxymethylfurfural into the innovative fuels and chemicals, Renew. Sust. Energ. Rev. 74 (2017) 230–257, https://doi.org/10.1016/J.RSER.2017.02.042.
[3] Y. Zheng, J. Wang, D. Wang, Z. Zheng, Advanced catalytic upgrading of biomass pyrolysis vapor to bio-aromatics hydrocarbon: a review, Appl. Energy Combust. Sci. 10 (2022), 100061, https://doi.org/10.1016/J.JAECS.2022.100061.
[4] S.N. Naik, V.V. Goud, P.K. Rout, A.K. Dalai, Production of first and second generation biofuels: a comprehensive review, Renew. Sust. Energ. Rev. 14 (2010) 578–597, https://doi.org/10.1016/J.RSER.2009.10.003.
[5] S. Hull, J. Arntzen, C. Blaser, A. Crossley, R. Jackson, E. Lobner, L. Paine, D. Sample, J. Vandenbrook, S. Ventura, S. Wallilng, J. Widholm, C. Williams, Wisconsin Sustainable Planting and Harvest Guidelines for Nonforest Biomass, 2014.
[6] L. Aguiar, F. Márquez-Montesinos, A. Gonzalo, J.L. Sánchez, J. Arauzo, Influence of temperature and particle size on the fixed bed pyrolysis of orange peel residues, J. Anal. Appl. Pyrolysis 83 (2008) 124–130, https://doi.org/10.1016/J.JAAP.2008.06.009.
[7] R. Singh, B.B. Krishna, J. Kumar, T. Bhaskar, Opportunities for utilization of non-conventional energy sources for biomass pretreatment, Bioresour. Technol. 199 (2016) 398–407, https://doi.org/10.1016/J.BIORTECH.2015.08.117.
[8] E. Santillan-Jimenez, M. Crocker, Catalytic deoxygenation of fatty acids and their derivatives to hydrocarbon fuels via decarboxylation/decarbonylation, J. Chem. Technol. Biotechnol. 87 (2012) 1041–1050, https://doi.org/10.1002/JCTB.3775.
[9] A. Demirbas, Biofuels securing the planet's future energy needs, Energy Convers. Manag. 50 (2009) 2239–2249, https://doi.org/10.1016/J.ENCONMAN.2009.05.010.
[10] J. Zakzeski, P.C.A. Bruijnincx, A.L. Jongerius, B.M. Weckhuysen, The Catalytic Valorization of Lignin for the production of Renewable Chemicals, Chem. Rev. 110 (2010) 3552–3599, https://doi.org/10.1021/cr900354u.
[11] P.J. Wild, W.J.J. De Huijgen, H.J. Heeres, P.J.D. Wild, W.J.J. Heeres, P.J. De Wild, W.J.J. Huijgen, Pyrolysis of wheat straw-derived organosolv lignin, J. Anal. Appl. Pyrolysis 93 (2012) 95–103, https://doi.org/10.1016/j.jaap.2011.10.002.
[12] X. Wang, Q. Fan, S. Yu, Z. Chen, Y. Ai, Y. Sun, A. Hobiny, A. Alsaedi, X. Wang, Retraction notice to "High sorption of U(VI) on graphene oxides studied by batch experimental and theoretical calculations" [Chem. Eng. J. 287 (2015) 448–455], Chem. Eng. J. 390 (2020), 124272, https://doi.org/10.1016/J.CEJ.2020.124272.
[13] D.C. Palacio Lozano, H.E. Jones, T. Ramirez Reina, R. Volpe, M.P. Barrow, Unlocking the potential of biofuels via reaction pathways in van Krevelen diagrams, Green Chem. 23 (2021) 8949–8963, https://doi.org/10.1039/D1GC01796A.
[14] L. Nie, P.M. De Souza, F.B. Noronha, W. An, T. Sooknoi, D.E. Resasco, Selective conversion of m-cresol to toluene over bimetallic Ni–Fe catalysts, J. Mol. Catal. A-Chem. 388–389 (2014) 47–55, https://doi.org/10.1016/J.MOLCATA.2013.09.029.
[15] B. Peng, C. Zhao, S. Kasakov, S. Foraita, J.A. Lercher, Manipulating catalytic pathways: deoxygenation of palmitic acid on multifunctional catalysts, Chem. Eur J. 19 (2013) 4732–4741, https://doi.org/10.1002/CHEM.201203110.
[16] J.G. Immer, H.H. Lamb, Fed-batch Catalytic Deoxygenation of Free Fatty Acids, Energy Fuel 24 (2010) 5291–5299, https://doi.org/10.1021/EF100576Z.
[17] D.C. Elliott, H. Wang, M. Rover, L. Whitmer, R. Smith, R. Brown, Hydrocarbon liquid production via catalytic hydroprocessing of phenolic oils fractionated from fast pyrolysis of Red Oak and Corn Stover, ACS Sustain. Chem. Eng. 3 (2015) 892–902, https://doi.org/10.1021/ACSSUSCHEMENG.5B00015/ASSET/IMAGES/MEDIUM/SC-2015-00015P_0009.GIF.
[18] R.M. Bown, M. Joyce, Q. Zhang, T.R. Reina, M.S. Duyar, Identifying commercial opportunities for the reverse water gas shift reaction, Energy Technol. 9 (2021) 2100554, https://doi.org/10.1002/ENTE.202100554.
[19] W. Jin, L. Pastor-Pérez, D.K. Shen, A. Sepúlveda-Escribano, S. Gu, T. Ramirez Reina, Catalytic Upgrading of Biomass Model Compounds: Novel Approaches and Lessons Learnt from Traditional Hydrodeoxygenation – a Review, ChemCatChem. 11 (2019) 924–960, https://doi.org/10.1002/CCTC.201801722.
[20] W. Jin, L. Pastor-Pérez, J. Yu, J.A. Odriozola, S. Gu, T.R. Reina, Cost-effective routes for catalytic biomass upgrading, Curr. Opin. Green Sustain. Chem. 23 (2020) 1–9, https://doi.org/10.1016/J.COGSC.2019.12.008.
[21] W. Jin, J. Luis Santos, L. Pastor-Perez, S. Gu, M. Angel Centeno, T. Ramirez Reina, Noble Metal Supported on Activated Carbon for "Hydrogen Free" HDO Reactions: Exploring Economically Advantageous Routes for Biomass Valorisation, ChemCatChem. 11 (2019) 4434–4441, https://doi.org/10.1002/cctc.201900841.
[22] W. Jin, L. Pastor-Pérez, J.J. Villora-Picó, A. Sepúlveda-Escribano, S. Gu, T.R. Reina, Investigating New Routes for Biomass Upgrading: "H2-Free" Hydrodeoxygenation using Ni-based Catalysts, ACS Sustain. Chem. Eng. 7 (2019) 16041–16049, https://doi.org/10.1021/ACSSUSCHEMENG.9B02712/ASSET/IMAGES/LARGE/SC9B02712_0008.JPEG.
[23] J.L. Santos, P. Mäki-Arvela, J. Wärnå, A. Monzón, M.A. Centeno, D.Y. Murzin, Hydrodeoxygenation of vanillin over noble metal catalyst supported on biochars: Part II: Catalytic behaviour, Appl. Catal. B Environ. 268 (2020), 118425, https://doi.org/10.1016/J.APCATB.2019.118425.
[24] W. Li, H. Wang, X. Wu, L.E. Betancourt, C. Tu, M. Liao, X. Cui, F. Li, J. Zheng, R. Li, Ni/hierarchical ZSM-5 zeolites as promising systems for phenolic bio-oil upgrading: Guaiacol hydrodeoxygenation, Fuel. 274 (2020), 117859, https://doi.org/10.1016/J.FUEL.2020.117859.
[25] D. Gao, C. Schweitzer, H.T. Hwang, A. Varma, Conversion of guaiacol on noble metal catalysts: Reaction performance and deactivation studies, Ind. Eng. Chem. Res. 53 (2014) 18658–18667, https://doi.org/10.1021/IE500495Z/ASSET/IMAGES/MEDIUM/IE-2014-00495Z_0008.GIF.
[26] S. Parrilla-Lahoz, W. Jin, L. Pastor-Pérez, D. Carrales-Alvarado, J.A. Odriozola, A. B. Dongil, T.R. Reina, Guaiacol hydrodeoxygenation in hydrothermal conditions using N-doped reduced graphene oxide (RGO) supported Pt and Ni catalysts: seeking for economically viable biomass upgrading alternatives, Appl. Catal. A Gen. 611 (2021), 117977, https://doi.org/10.1016/J.APCATA.2020.117977.
[27] L. Pastor-Pérez, W. Jin, J.J. Villora-Picó, Q. Wang, M. Mercedes Pastor-Blas, A. Sepúlveda-Escribano, T.R. Reina, "H2-free" demethoxylation of guaiacol in subcritical water using Pt supported on N-doped carbon catalysts: a cost-effective strategy for biomass upgrading, J. Energy Chem. 58 (2021) 377–385, https://doi.org/10.1016/j.jechem.2020.10.045.
[28] W. Jin, J.L. Santos, L. Pastor-Perez, S. Gu, M.A. Centeno, T.R. Reina, Noble Metal Supported on Activated Carbon for "Hydrogen Free" HDO Reactions: Exploring Economically Advantageous Routes for Biomass Valorisation, ChemCatChem. 11 (2019) 4434–4441, https://doi.org/10.1002/CCTC.201900841.
[29] I. Barroso-Martín, D. Ballesteros-Plata, A. Infantes-Molina, M.O. Guerrero-Pérez, J. Santamaría-González, E. Rodríguez-Castellón, An overview of catalysts for the hydrodeoxygenation reaction of model compounds from lignocellulosic biomass, IET Renew. Power Gener. (2022), https://doi.org/10.1049/RPG2.12477.
[30] K.A. Cychosz, R. Guillet-Nicolas, J. García-Martínez, M. Thommes, Recent advances in the textural characterization of hierarchically structured nanoporous materials, Chem. Soc. Rev. 46 (2017) 389–414, https://doi.org/10.1039/C6CS00391E.
[31] J.L. Santos, C. Megías-Sayago, S. Ivanova, M.Á. Centeno, J.A. Odriozola, Functionalized biochars as supports for Pd/C catalysts for efficient hydrogen production from formic acid, Appl. Catal. B Environ. 282 (2021), 119615, https://doi.org/10.1016/J.APCATB.2020.119615.
[32] S. Gautam, Sahoo, Experimental investigation on different activated carbons as adsorbents for CO2 capture, Therm. Sci. Eng. Prog. 33 (2022), 101339, https://doi.org/10.1016/J.TSEP.2022.101339.
[33] M.A. Centeno, T. Ramírez Reina, S. Ivanova, O.H. Laguna, J.A. Odriozola, Au/CeO2 catalysts: structure and CO Oxidation activity, Catalysts. 6 (2016) 158, https://doi.org/10.3390/catal6100158.
[34] S.H. Oh, R.M. Sinkevitch, Carbon Monoxide Removal from Hydrogen-Rich fuel Cell Feedstreams by Selective Catalytic Oxidation, J. Catal. 142 (1993) 254–262, https://doi.org/10.1006/JCAT.1993.1205.
[35] K.M.S. Khalil, M. Khairy, O.A.S. Allam, M.K. Khalil, Formation of improved activated carbons from sugarcane bagasse as environmental materials for adsorption of phenolic pollutants, Int. J. Environ. Sci. Technol. 19 (2022) 3103–3116, https://doi.org/10.1007/s13762-021-03382-3.
[36] J. Gandara-Loe, E. Portillo, J.A. Odriozola, T.R. Reina, L. Pastor-Pérez, K-promoted Ni-based catalysts for gas-phase CO2 conversion: catalysts design and process

modelling validation, Front. Chem. 9 (2021) 1005, https://doi.org/10.3389/FCHEM.2021.785571/BIBTEX.
[37] L. Pastor-Pérez, F. Baibars, E. Le Sache, H. Arellano-García, S. Gu, T.R. Reina, CO2 valorisation via reverse Water-Gas Shift reaction using advanced Cs doped Fe-Cu/Al2O3 catalysts, J. CO2 Util. 21 (2017) 423–428, https://doi.org/10.1016/J.JCOU.2017.08.009.
[38] F. Su, L. Lv, F. Yin Lee, T. Liu, A.I. Cooper, X. Song Zhao, Thermally Reduced Ruthenium Nanoparticles as a Highly active Heterogeneous Catalyst for Hydrogenation of Monoaromatics, J. Am. Chem. Soc. 129 (2007) 14213–14223, https://doi.org/10.1021/ja072697v.
[39] S.-Y. Huang, C.-M. Chang, C.-T. Yeh, Promotion of platinum–ruthenium catalyst for electro-oxidation of methanol by ceria, J. Catal. 241 (2006) 400–406, https://doi.org/10.1016/j.jcat.2006.04.020.
[40] NIST X-ray Photoelectron Spectroscopy Database, NIST Standard Reference Database Number 20, National Institute of Standards and Technology, Gaithersburg MD 20899 (2000), https://doi.org/10.18434/T4T88K.
[41] Oxygen, XPS Periodic Table | Thermo Fisher Scientific - ES. https://www.thermofisher.com/es/es/home/materials-science/learning-center/periodic-table/non-metal/oxygen.html, 2023 (accessed October 7, 2022).
[42] C. Zhang, W. Lv, Q. Yang, Y. Liu, Graphene supported nano particles of Pt-Ni for CO oxidation, Appl. Surf. Sci. 258 (2012) 7795–7800, https://doi.org/10.1016/J.APSUSC.2012.03.131.
[43] S. López-Rodríguez, A. Davó-Quiñonero, E. Bailón-García, D. Lozano-Castelló, A. Bueno-López, Effect of Ru loading on Ru/CeO2 catalysts for CO2 methanation, Mol. Catal. 515 (2021), https://doi.org/10.1016/J.MCAT.2021.111911.
[44] R. Prins, Hydrogen spillover. Facts and fiction, Chem. Rev. 112 (2012) 2714–2738, https://doi.org/10.1021/CR200346Z/ASSET/IMAGES/MEDIUM/CR-2011-00346Z_0024.GIF.
[45] M. Xiong, Z. Gao, Y. Qin, Spillover in heterogeneous catalysis: new insights and opportunities, ACS Catal. 11 (2021) 3159–3172, https://doi.org/10.1021/ACSCATAL.0C05567/ASSET/IMAGES/LARGE/CS0C05567_0009.JPEG.
[46] X. Wang, P. Wu, Z. Wang, L. Zhou, Y. Liu, H. Cheng, M. Arai, C. Zhang, F. Zhao, Chlorine-Modified Ru/TiO 2 Catalyst for Selective Guaiacol Hydrodeoxygenation, 2021, https://doi.org/10.1021/acssuschemeng.0c07292.
[47] L. Rivoira, M.L. Martínez, A. Beltramone, Hydrodeoxygenation of guaiacol over Pt-Ga-mesoporous catalysts, Microporous Mesoporous Mater. 312 (2021), https://doi.org/10.1016/J.MICROMESO.2020.110815.
[48] M. Zhou, F. Ge, J. Li, H. Xia, J. Liu, J. Jiang, C. Chen, J. Zhao, X. Yang, Catalytic hydrodeoxygenation of guaiacol to cyclohexanol over bimetallic NiMo-MOF-derived catalysts, Catalysts. 12 (2022) 371, https://doi.org/10.3390/CATAL12040371/S1.
[49] E.H. Lee, R. Su Park, H. Kim, S.H. Park, S.C. Jung, J.K. Jeon, S.C. Kim, Y.K. Park, Hydrodeoxygenation of guaiacol over Pt loaded zeolitic materials, J. Ind. Eng. Chem. 37 (2016) 18–21, https://doi.org/10.1016/J.JIEC.2016.03.019.
[50] Y. He, Y. Bie, J. Lehtonen, R. Liu, J. Cai, Hydrodeoxygenation of guaiacol as a model compound of lignin-derived pyrolysis bio-oil over zirconia-supported Rh catalyst: Process optimization and reaction kinetics, Fuel. 239 (2019) 1015–1027, https://doi.org/10.1016/J.FUEL.2018.11.103.
[51] S. Parrilla-Lahoz, W. Jin, L. Pastor-Pérez, M.S. Duyar, L. Martínez-Quintana, A. B. Dongil, T.R. Reina, Multicomponent graphene based catalysts for guaiacol upgrading in hydrothermal conditions: Exploring “H2-free” alternatives for bio-compounds hydrodeoxygenation, Catal. Today (2023), https://doi.org/10.1016/J.CATTOD.2023.01.027.
[52] W. Jin, L. Pastor-Pérez, J.J. Villora-Picó, M.M. Pastor-Blas, J.A. Odriozola, A. Sepúlveda-Escribano, T.R. Reina, In-situ HDO of guaiacol over nitrogen-doped activated carbon supported nickel nanoparticles, Appl. Catal. A Gen. 620 (2021), 118033, https://doi.org/10.1016/J.APCATA.2021.118033.